A&A 406, 65–73 (2003)
DOI: 10.1051/0004-6361:20030793

Astronomy & Astrophysics

Outflowing material in the z_{em} = 4.92 BAL QSO SDSS J160501.21–011220.0⋆

N. Gupta[1], R. Srianand[2], P. Petitjean[3,4], and C. Ledoux[5]

[1] NCRA, Post Bag 3, Ganeshkhind, Pune 411 007, India
e-mail: neeraj@ncra.tifr.res.in
[2] IUCAA, Post Bag 4, Ganeshkhind, Pune 411 007, India
e-mail: anand@iucaa.ernet.in
[3] Institut d'Astrophysique de Paris – CNRS, 98bis Boulevard Arago, 75014 Paris, France
[4] LERMA, Observatoire de Paris, 61 rue de l'Observatoire, 75014 Paris, France
e-mail: petitjean@iap.fr
[5] European Southern Observatory, Alonso de Córdova 3107, Casilla 19001, Vitacura, Santiago, Chile
e-mail: cledoux@eso.org

Received 17 January 2003 / Accepted 6 May 2003

Abstract. We present the analysis of broad absorption lines (BALs) seen in the spectrum of the $z_{em} \simeq 4.92$ QSO SDSS J160501.21-011220.0. Our high spectral resolution UVES spectrum shows two well-detached absorption line systems at z_{abs} = 4.685 and 4.855. The system at z_{abs} = 4.855 covers the background source completely, suggesting that the gas is located outside the broad emission line region. On the contrary, the system at z_{abs} = 4.685, which occults only the continuum source, has a covering factor of the order of 0.9. Physical conditions are investigated in the BAL system at z_{abs} = 4.855 using detailed photoionization models. The observed H I absorption line together with the limits on C II and Si II absorptions suggest that $16 < \log N(\mathrm{H\,I})\,(\mathrm{cm}^{-2}) < 17$ in this system. Comparison with models show that the observed column densities of N V , Si IV and C IV in this system require that nitrogen is underabundant by more than a factor of 3 compared to silicon if the ionizing radiation is similar to a typical QSO spectrum. This is contrary to what is usually derived for the emission line gas in QSOs. We show that the relative suppression in the N V column density can be explained for Solar abundance ratios or abundance ratios typical of Starburst abundances if an ionizing spectrum devoid of X-rays is used instead. Thus, if the composition of BAL is like that of the emission line regions it is most likely that the cloud sees a spectrum devoid of X-rays similar to what we observe from this QSO. This is consistent with the fact that none of our models have high Compton optical depths to remove X-rays from the QSO. Similar arguments lead to the conclusion that the system at z_{abs} = 4.685 as well is not Compton thick. Using simple Eddington arguments we show that the mass of the central black hole is $\sim 7.1 \times 10^8\ M_\odot$. This suggests that the accretion onto a seed black hole must have started as early as $z \sim 11$.

Key words. quasars: absorption lines – quasars: individual: SDSS J160501.21-011220.0

1. Introduction

Broad absorption line systems (BALs) seen in the spectra of QSOs are characterized by absorption features with large velocity widths ($\Delta v \sim$ a few 1000 km s^{-1}) and, usually, high ionization states (Turnshek et al. 1988; Weymann et al. 1991). The gas giving rise to BALs is believed to be material ejected by the quasar and still located very close to the central regions. Thus studying metallicities in the absorbing gas is a direct probe of the chemical enrichment in the very central regions of AGNs (see Hamann & Ferland 1999 for the review). The associated absorption line systems by and large show high metallicities with a tendency for nitrogen to be over-abundant with respect to oxygen and other $\alpha-$process elements (e.g. Petitjean et al. 1994; Korista et al. 1996; Hamann 1997; Petitjean & Srianand 1999). Detailed studies of emission line properties of $z \geq 4$ QSOs have revealed Super-Solar metallicities in the line emitting gas in broad line regions (BLR), suggesting very rapid star formation process (e.g. Hamann & Ferland 1992; Dietrich et al. 2003). However, no such metallicity estimates at such high redshifts based on absorption lines using echelle spectra are available.

Unlike the case of most normal galaxies, it is believed that the high metal enrichment usually observed in QSOs takes place in less than a few 10^8 years through rapid star formation, similar to what is expected to happen in the center of ellipticals (Hamann & Ferland 1993; Matteucci & Padovani 1993). Thus,

Send offprint requests to: R. Srianand

⋆ Based on observations carried out at the European Southern Observatory (ESO) under programmes 67.A-0078 and 69.A-0457 with the UVES spectrograph installed at the Nasmyth focus B of the VLT 8.2m telescope, unit Kueyen, on Cerro Paranal in Chile.

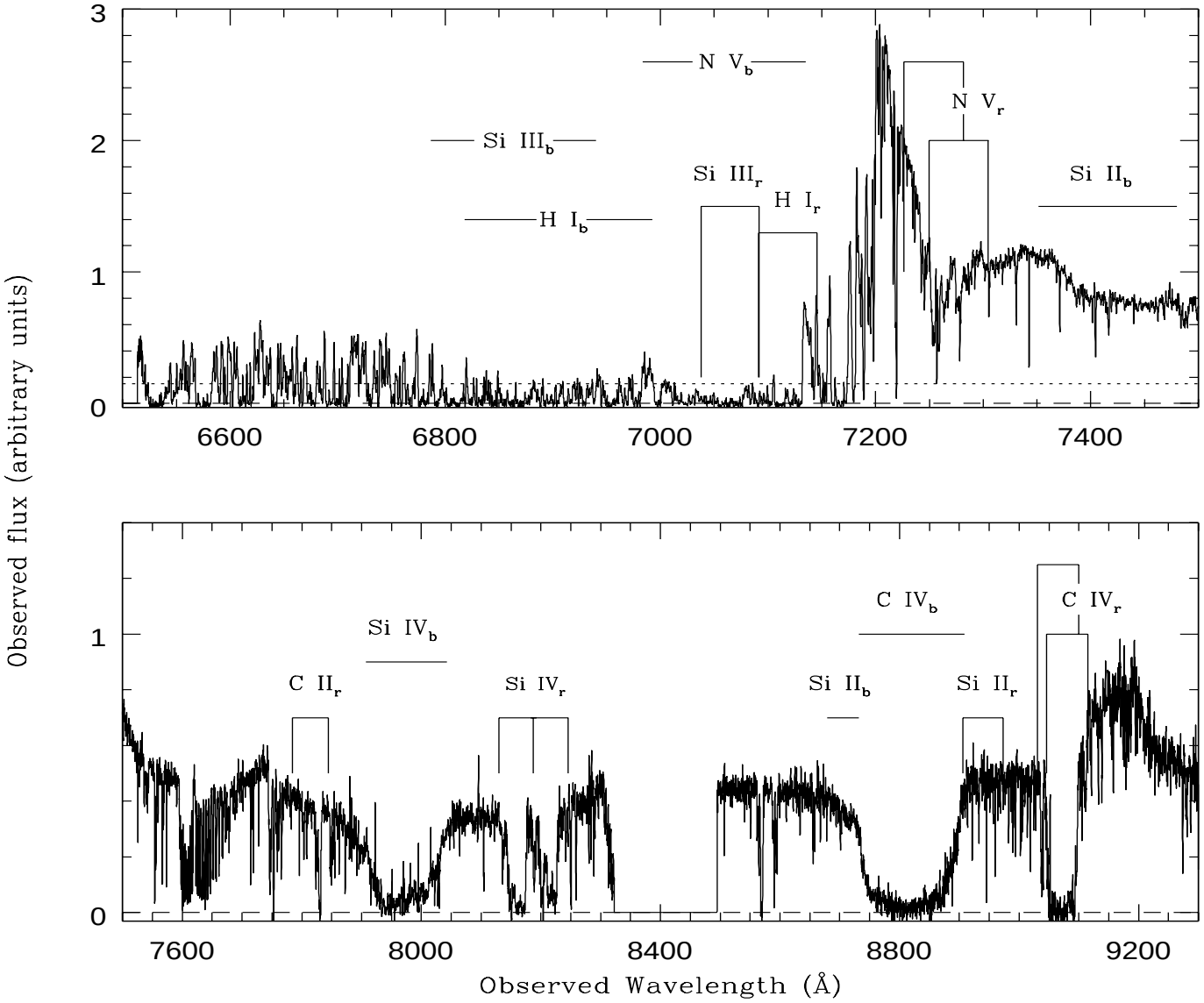

Fig. 1. UVES spectrum of the $z_{em} = 4.92$ QSO SDSS J160501.21-011220. Two well detached BAL features are seen covering the redshift ranges 4.62−4.75 and 4.83−4.88. We denote them as blue and red systems respectively. The expected positions of different lines (with sub-scripts *r* and *b* denoting red and blue respectively) are marked with solid lines. The horizontal dotted line in the top panel gives the mean transmitted flux computed over the Lyα forest in the wavelength range 6550−6800 Å that is not affected by the BAL absorption lines.

studying BAL QSOs at $z_{em} \geq 5$, where the age of the Universe is $t \leq 1.07 \times 10^9$ yr (for $H_o = 75$ km s^{-1} Mpc^{-1}, $\Omega_\Lambda = 0.70$, $\Omega_m = 0.30$), is important for understanding the star-formation history at a time close to the epoch of reionization and possibly also for constraining cosmological parameters. In the initial list of SDSS QSOs (Fan et al. 2000) there are few QSOs at $z \geq 4$ with associated absorption lines. We obtained a UVES spectrum of the QSO SDSS J160501.21-011220.0, the highest redshift BAL QSO known at that time, with the aim to study the outflowing gas in detail.

In order to derive a realistic estimate of the absorbing gas metallicity one needs to have a good handle on the ionization corrections. Associated systems being close to the QSO are most probably ionized by the QSO light rather than the diffuse intergalactic background. However, the ionizing spectrum from the BAL QSOs is poorly known. It is known that BAL QSOs are under-luminous in X-rays (Bregman 1984; Singh et al. 1987; Green & Mathur 1996). Recent, deep Chandra observations have shown that the optical to X-ray spectral index, α_{OX}, measured for BAL QSOs is systematically lower than that of non-BAL QSOs (Green et al. 2001). It is not clear whether this X-ray weakness is due to the QSO being intrinsically X-ray quiet (i.e., this is a property of the central engine) or due to line-of-sight absorption (i.e., radiative transfer effects). Using a complete sample of optically selected QSOs, Brandt et al. (2000) have shown a significant anti-correlation between α_{OX} and the total equivalent width of the C IV absorption lines. In addition it is noticed that the emission line properties of the BAL and non-BAL QSOs are very similar even though the observed X-ray properties differ significantly (Weymann et al. 1991; Korista et al. 1993). Thus, it is most likely that the relative X-ray weakness of BAL QSOs is due to intrinsic absorption.

It must be noted that all existing models of BAL systems assume a standard QSO spectrum. However, estimated metallicities will be different if the intrinsic $\alpha_{\rm OX}$ is different from that of a typical QSO spectrum. Indeed, Srianand & Petitjean (2000) have shown that the inferred metallicities decrease with decreasing values of $\alpha_{\rm OX}$. Also, if the absorption is responsible for the suppression of X-rays then it is important to investigate whether it is caused by the gas responsible for the BAL troughs (common absorbers) or by a distinct gas component. It is likely that the common absorber picture is correct for the BAL towards PHL 5200 (Mathur et al. 1995) and that a distinct Compton thick screen is required for the BAL towards PG 0946+301 (Gallagher et al. 1999; Mathur et al. 2000; see also Kraemer et al. 2002).

In this paper we present a detailed analysis of two well-detached BAL outflow components that are seen in the spectrum of QSO J160501.21-011220.0 ($z_{\rm em}$ = 4.92). Details of the observations are discussed in Sect. 2 which is followed by the description of the BALs and column density estimates in Sect. 3. In Sect. 4 we investigate the physical conditions of the gas. The results are summarised in Sect. 5.

2. Observations and data reduction

The Ultraviolet and Visible Echelle Spectrograph (UVES; Dekker et al. 2000), installed at the ESO VLT 8.2 m telescope, Kueyen unit, on Mount Paranal in Chile, was used on June 15-17, 2001, to obtain high resolution spectra of QSO J 160501.21−011220.0. A non-standard setting with cross-disperser #4 and central wavelength 8420 Å was used in the Red arm of UVES. Full wavelength coverage was obtained this way from 6514 to 8300 Å and from 8494 to 9300 Å, accounting for the gap between the two Red-arm CCDs. The CCD pixels were binned 2 × 3 (namely, twice in the spatial direction and three times in the dispersion direction) and the slit width was either fixed to 1.″2 or 1.″5, yielding an overall spectral resolution $R \sim 30\,000$. The total integration time 3h30min was split into 3 exposures. The data were reduced in the dedicated context of MIDAS[1], the ESO data reduction system, using the UVES pipeline (Ballester et al. 2000) in an interactive mode. The main characteristics of the pipeline is to perform a precise inter-order background subtraction for science frames and master flat-fields, and an optimal extraction of the object signal rejecting a number of cosmic ray impacts and subtracting the sky spectrum simultaneously. The pipeline products are checked step by step. The wavelength scale of the spectra reduced by the pipeline was then converted to vacuum-heliocentric values and individual 1-D exposures scaled, weighted and combined altogether using the NOAO *onedspec* package of the IRAF[2] software. During this process, the spectra were rebinned to 0.08 Å pix^{-1}. In order to increase the signal-to-noise ratio in this near-IR part of the optical range (and as the lines of interest are broad), we applied a Gaussian filter smoothing with two pixel *FWHM* and get an effective spectral resolution of ∼12 km s^{-1}. The resulting signal-to-noise ratio per pixel is of the order of 20 or more over most of the wavelength range considered here. The final spectrum is shown in Fig. 1.

The continuum fitting in the red side of the Lyα emission was done using a smooth low order polynomial considering only the absorption free regions. In the Lyman-α forest, we approximated the QSO spectrum by a powerlaw, $f_\nu \propto \nu^{-0.6}$, that we fitted on the low-dispersion SDSS spectrum made available to us by Dr. Fan. The normalization of the power-law was done using the flux in the region between the C IV and Si IV emission lines. In our normalised spectrum the mean Lyα transmission flux in the redshift range z = 4.39 to z = 4.60 (that is not contaminated by any BAL absorption lines) is 0.15. This is consistent with the values derived in the same redshift range using non-BAL QSOs (Becker et al. 2001).

3. Broad absorption line systems

Based on the unabsorbed C IV emission line we estimate the emission redshift of the QSO to be $z_{\rm em}$ = 4.92. Two well detached absorption line systems are identified based on the C IV and Si IV absorptions over the redshift ranges, $z_{\rm abs}$ = 4.83−4.88 and $z_{\rm abs}$ = 4.62−4.75, respectively. For mean redshifts $z_{\rm abs}$ = 4.855 and 4.685, this corresponds to ejection velocities of ≈3330 km s^{-1} and ≈12 160 km s^{-1}. The spectrum in the Lyman-α forest is heavily affected by the high Lyα opacity of the intergalactic medium. Even though excess absorption is seen at the expected positions of BAL absorption lines (see Fig. 1) it is difficult to estimate column densities in this region. Therefore, in the following sections we use only lines observed on the red side of the Lyα emission line to investigate the physical conditions in the outflowing gas.

3.1. The red component at $z_{\rm abs}$ = 4.855

The absorption trough in this component is ∼2000 km s^{-1} wide. The absorption profiles of different transitions centered at $z_{\rm abs}$ = 4.855 are shown in Fig. 2. The absorption profile of the Si IV doublet that is comparatively less saturated than that of the C IV doublet suggests the presence of 2 relatively narrow components denoted by l1 and l2 and 3 broad subcomponents denoted by a, b and c. While Lyα and C IV are detected in all these components, N V absorption is detected only in the broad subcomponents (see Fig. 2).

All the obviously saturated absorption lines have zero residuals (C IV and Lyman-α, see Fig. 2). The covering factor of the gas is therefore unity. In case of complete coverage the observed residual intensities R_1 and R_2 in the first and second member of the doublet are related as $R_1 = R_2^2$ (see Srianand & Shankarnaraynan 1999). Indeed, even though part of the N V absorption line is contaminated by atmospheric absorption (see Fig. 3), the velocity ranges in the profiles that are free of blending are consistent with complete coverage (see top panel in Fig. 3). As emission in this wavelength range is contributed by both continuum and broad emission lines the corresponding

[1] MIDAS: Munich Image Data Analysis System, trademark of the European Southern Observatory (ESO).

[2] IRAF: The Image Reduction and Analysis Facility is distributed by the National Optical Astronomy Observatories, which is operated by the Association of Universities for Research in astronomy, Inc. (AURA), under cooperative agreement with the National Science Foundation.

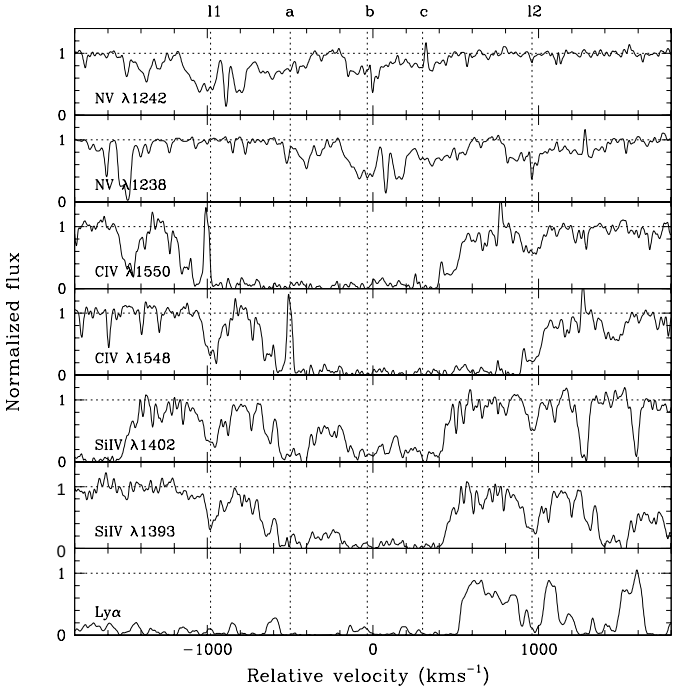

Fig. 2. Velocity plots of the red absorption line system centered at z_{abs} = 4.855. We identify 5 distinct components based on the Si IV and C IV profiles (marked with vertical dotted lines). Detection of Lyα line in this system is unambiguous as the profile just follows the well detached Si IV absorption line at least from 0 to 600 km s^{-1}.

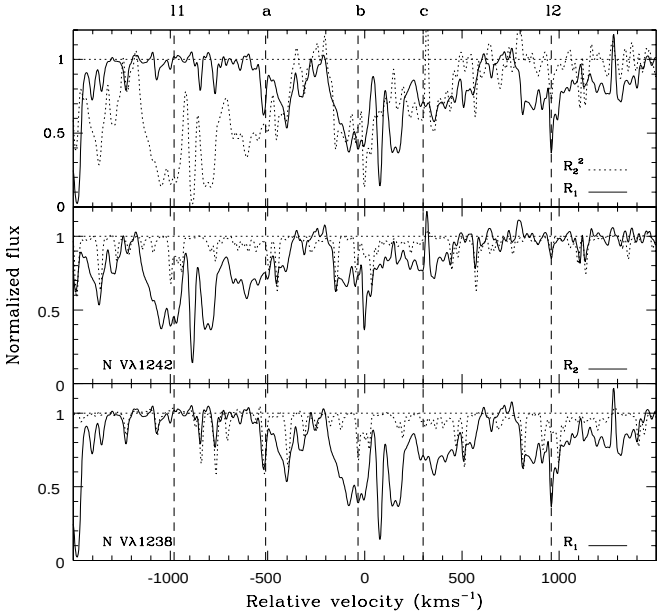

Fig. 3. Velocity plots of N V doublets centered at z_{abs} = 4.855. R_1 and R_2 are the residual intensities in the first and second lines of the doublet. Vertical dotted lines show the subcomponents l1, a, b, c and l2 respectively. In the lower two panels the dotted profiles give the atmospheric lines seen toward QSO 1122−1628. In the top panel we overplot the two N V profiles after appropriately scaling (see text) the N Vλ1242 line assuming complete coverage. The good matching of profiles suggests that N V absorption line covers the background source completely.

absorbing gas has to be located outside the broad line region (BLR). As the N V lines are weak we can derive the N V column densities. However, due to saturation effects, we can determine only lower limits for C IV and H I column densities. It can be seen in Fig. 2 that Si IVλ1402 is only partly saturated which means that, although very uncertain, we can estimate the corresponding column density. We use also the Si IVλ1402 profile as a template to determine upper limits on the column densities of non detected species (see below).

The column density in each velocity pixel was obtained using the relation

$$N(v) = 3.768 \times 10^{+14}\ \tau / f\lambda\ \mathrm{cm}^{-2}\ \mathrm{km}^{-1}\mathrm{s} \qquad (1)$$

where, τ, f and λ are the optical depth, oscillator strength and rest wavelength respectively. The total column density is obtained by integrating $N(v)$ over the velocity range −1120 to 1160 km s^{-1}. The results are presented in Table 1. Rest wavelengths and oscillator strengths used here are taken from Verner et al. (1994). The two lines of the C IV doublet are blended and we use an effective oscillator strength, $f = f_1 + f_2$, and mean wavelength, $(\lambda_1 + \lambda_2)/2$, to compute the lower limit on the column density. In the case of N V, we use the N Vλ1238 line for component a and N Vλ1242 line for components b and c that are free of blending. Contamination by atmospheric features (see Fig. 3) is corrected by carefully masking the atmospheric contamination using the normalised spectrum of Q 1122−1628.

Singly ionized species such as Si II, C II and Al II are absent and the spectrum at the expected position of Al III lines is unfortunately very noisy. As said above, we evaluate upper limits for column densities of the latter species using

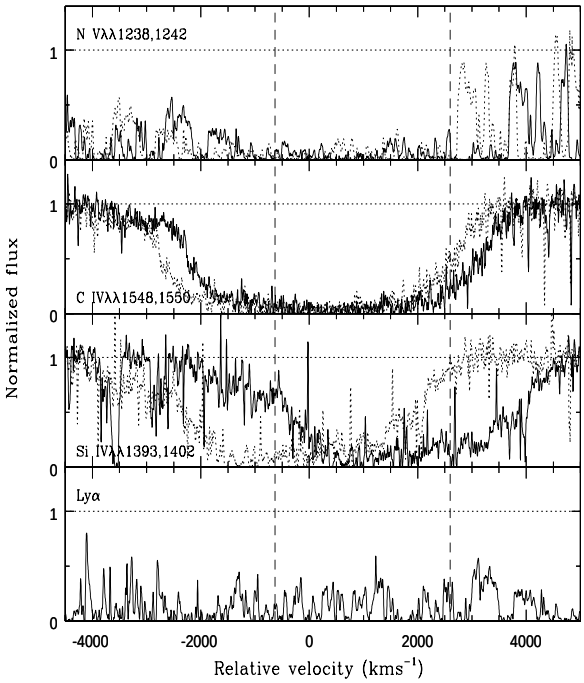

Fig. 4. Velocity plots for the blue component centered at z_{abs} = 4.685. Second member of the doublets is overlaid as a dotted line. Vertical dashed lines mark the velocity range over which Si IV absorption line is seen. Note that C IV absorption is seen over a larger velocity range. The non-zero residual flux at the expected position of Lyα absorption is used for obtaining the upper limit on the H I column density.

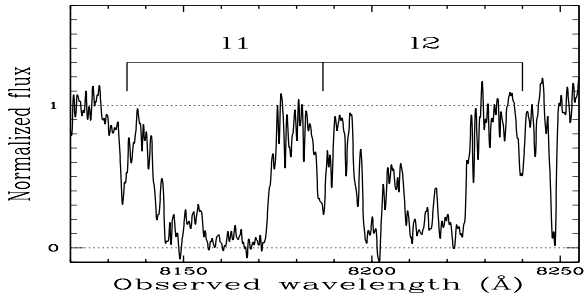

Fig. 5. Region of the spectrum containing the Si IV trough of the red BAL component at $z_{abs} \sim 4.855$. Note that systems l1 and l2 have a velocity separation equal to that of the Si IV doublet splitting suggesting the presence of line-locking in the system.

Table 1. Column densities estimated using apparent optical depth method with complete coverage.

z_{abs}	species	log N (cm^{-2})
4.855	H I	≥15.67
	C II	≤14.21
	C IV	≥15.64
	Si II	≤14.13
	Si IV	≥15.33
	N V	14.63–14.71
4.685	H I	≤ 16.00
	C IV	≥15.94
	Si II	≤14.73
	Si IV	≥15.40

the Si IVλ1402 profile (which is not completely saturated and least affected by atmospheric contamination) extending from −1120 to 1160 km s^{-1} as a template. The scaling factor $k = [N f\lambda]_{X^+}/[N f\lambda]_{\rm template}$ between the two optical depths $\tau_{\rm template}$ and τ_{X^+} for species X^+ is then obtained by minimizing

$$\alpha = \Sigma(\tau_{X^+} - k * \tau_{\rm template})^2. \quad (2)$$

For Si II and C II, k comes out to be 0.031 and 0.035 respectively. The corresponding upper limits on the column densities are given in Table 1. Note that the error in the column density of N V is mainly due to continuum placement uncertainties. We note that most of the atmospheric absorption seen in the expected wavelength range have consistent equivalent width. This suggests that our continuum fitting does not underpredict the absorption in the N V region. No flux is detected at the expected position of Si IIIλ1206 (see Fig. 1). However, we could not use this to derive a lower limit on Si III as the same region is contaminated by a probable N V absorption line from the blue component (see Fig. 4).

Finally we notice that the velocity separation between the two narrow components l1 and l2 of the red component is very close to the Si IV doublet splitting. This is shown in Fig. 5. This is consistent with growing evidence for line-locked flows and radiative acceleration in BAL systems (see Srianand et al. 2002 and references therein).

Table 2. Chemical compositions considered in the models.

	Solar	Starburst*		
Metal	1.0 $Z_\odot$	1.0 Z_{SB}	0.5 Z_{SB}	0.20 Z_{SB}
C	−3.44	−3.90	−4.22	−4.63
N	−4.03	−4.60	−5.34	−6.51
O	−3.13	−3.00	−3.30	−3.70
Si	−4.44	−4.43	−4.74	−5.14

* This form of Starburst abundances correspond to chemical evolution model M5a of Hamann & Ferland (1993).

3.2. The blue component at $z_{\rm abs} = 4.685$

The absorption profiles of different transitions centered at $z_{abs} = 4.685$ are shown in Fig. 4. Doublet partners for C IV and Si IV are partially blended together. The non-zero residual flux for the blended C IV$\lambda\lambda$1548,1550 corresponds to a covering factor, $f_c \geq 0.90$. It is interesting to note that the absorption is well detached from the emission line profile. Thus the partial coverage reflects either ≃10% contribution from the scattered light or partial coverage of the continuum source. Lower limits to column densities for the Si IV$\lambda\lambda$1393,1402 and C IV$\lambda\lambda$1548,1550 were obtained assuming full coverage (see Table 1). Doing otherwise would only increase these limits. Note that C IV absorption line extends over a larger velocity range as compared to Si IV absorption profile (see Fig. 4). Like in the red component, singly ionized species Si II and C II are not detected which indicates that the neutral hydrogen column density cannot be large (remember that metallicity in this kind of gas is usually large). N V may be present but its redshifted position in the Lyα forest overlaps with that of H I and Si III from the red component (see Fig. 1). The mean transmitted flux at the N V position is consistent with saturated absorption line.

In Fig. 4 the intervening Lyman-α forest is clearly observed over the whole range corresponding to the BAL H I Lyman-α trough. This means that the H I optical depth cannot be large except if the covering factor of H I is much smaller than that of C IV. This is not impossible (see e.g. Srianand et al. 2002) but would be surprising given the non detection of both C II and Si II. By comparing the mean transmission in this region with that devoid of BAL absorption lines we estimate that $\tau(v)$ for H I is less than 2. If we use the velocity range covered by the C IV profile (≃4000 km s^{-1}), we see that the H I column density can not much larger than 10^{16} cm^{-2}.

4. Discussion

4.1. Physical conditions in the outflowing gas

From the discussion in the previous Section, it is clear that constraints are not strong enough to probe the physical conditions in the blue component ($z_{abs} = 4.685$). We therefore mainly concentrate on the red component ($z_{abs} = 4.855$). Recent Chandra observations (Vignali et al. 2001) fail to detect X-rays from the QSO SDSS J160501.21-011220.0. As discussed before, the X-ray non-detection could be either due to large X-ray absorbing column density or a consequence of the QSO being intrinsically X-ray quiet. Indeed, there are already some reports that the X-ray continuum shapes of QSOs may evolve

Table 3. Summary of the photoionization models considered for the red component.

Model parameters				Allowed range in log U from		log(N(H(total)))*
Spectrum	Enrichment	Metallicity (Z)	log N(H I)*	Ratios	Observed N	
MF	Solar	0.5 $Z_\odot$, [Si/N] = 3.0[Si/N]$_\odot$	17.00	(−2.25, −2.15)	≈−2.2, −2.1	(19.99, 20.11)
BAL	”	1.0 $Z_\odot$	16.00	(−1.5, −1.1)	≈−1.1	20.00
”	”	1.5 $Z_\odot$	”	(−1.4, −0.95)	≈−1.0	19.90
”	”	0.05$_\odot$	17.00	(−1.7, −0.75)	≈−0.7	21.42
”	”	0.1 $Z_\odot$	”	(−1.7, −0.7)	(−0.9, −0.8)	(21.53, 21.62)
”	”	0.2 $Z_\odot$	”	(−1.65, −0.65)	≈−1.0	21.36
”	”	1.0 $Z_\odot$	”	(−1.4, −0.4)	–	–
”	Starburst	1.0 Z_{SB}	16.00	(−1.4, −0.65)	≈−0.7	20.30
”	”	5.0 Z_{SB}	”	(−1.4, −0.7)	≈(−1.0,−0.9)	(19.32, 19.41)
”	”	9.0Z_{SB}	”	(−1.15, −0.8)	≈−1.05	19.11
”	”	0.2 Z_{SB}	17.00	(−1.7, FP)	≈0.1	22.42
”	”	0.5 Z_{SB}	”	(−1.5, 0.1)	≈(−0.6, −0.5)	(21.60, 21.70)
”	”	1.0 Z_{SB}	”	(−1.3, 0.1)	≈−0.8	21.12

* in cm^{-2}

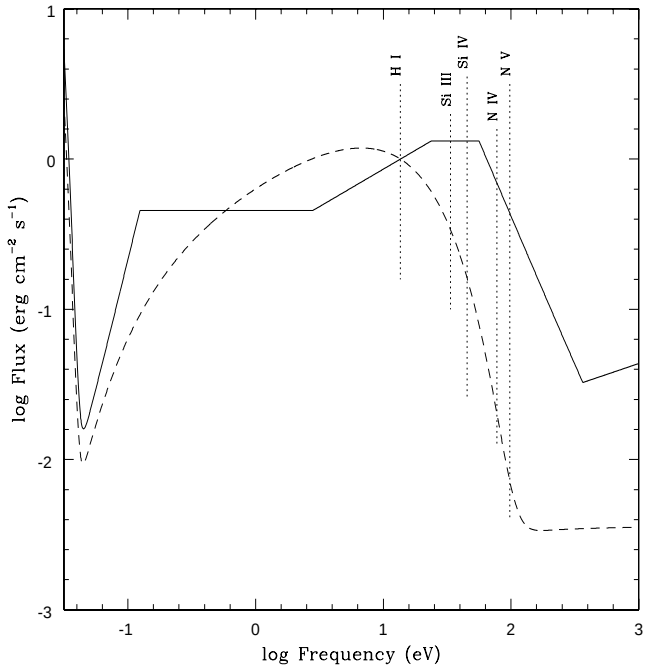

Fig. 6. The spectral energy distribution (SED) of the ionizing radiation. The continuous and dashed curves correspond to the SED of the MF and BAL spectrum respectively. The vertical dotted lines give the ionization potential of the different species we are interested in this study.

at $z \geq 2.5$ (e.g. Vignali et al. 1999; Blair et al. 2000; Vignali et al. 2003). Assuming that the lack of X-rays in this source is due to absorption, Vignali et al. (2001) infer that the X-ray non-detection for this object implies a total hydrogen column density of N(H(total)) $\geq 5.0 \times 10^{23}$ cm^{-2}, characteristic of low-ionization BAL QSOs at low redshift. Note that the limit on the X-ray flux further implies a small optical to X-ray spectral index, $\alpha_{ox} < -1.82$, for this object.

The absence of singly ionized species C II and Si II suggests that H I is optically thin at the Lyman limit. Thus, to probe the physical conditions in the red component, we run grids of photoionization models using Cloudy (Ferland 1996) in the range log N (H I) (cm^{-2}) ~ 10^{16} to 10^{17} cm^{-2}, considering the gas being ionized by either an unattenuated QSO spectrum given by Mathews & Ferland (1987) (hereafter MF spectrum; see Fig. 6) or a modified spectrum with little X-rays (hereafter BAL spectrum; see Fig. 6) mimicking attenuation of a typical QSO spectrum by a large column density of ionized gas (see below). The models are run for different chemical composition, either the Solar one or the so-called Starburst one (see Table 2). In all the models, the calculations are stopped when the total neutral hydrogen column density reaches the limit we set (log N(H I) (cm^{-2}) = 16 or 17).

The input parameters of the models, that reproduce the observed ratios as well as the column densities of individual species, are given in Table 3. The corresponding total hydrogen column density in the allowed range of ionization parameters is given in the last Column of the Table 3. Results for some selected models with different ionizing spectra and chemical composition for log N(H I) (cm^{-2}) = 17 are given in Fig. 7. In this figure we have plotted the column density of different species as a function of ionization parameter. The horizontal dotted lines mark limits on the observed column densities of Si II , Si IV , C II and C IV . The minimum and maximum of the allowed range for log U are marked with verticle dashed lines. The former is obtained using either of the ratios N(Si II)/N(Si IV) or N(C II)/N(C IV) and the latter is obtained from the observed N(N V)/N(Si IV) ratio for metallicities assumed in the model. The range of ionization parameters for

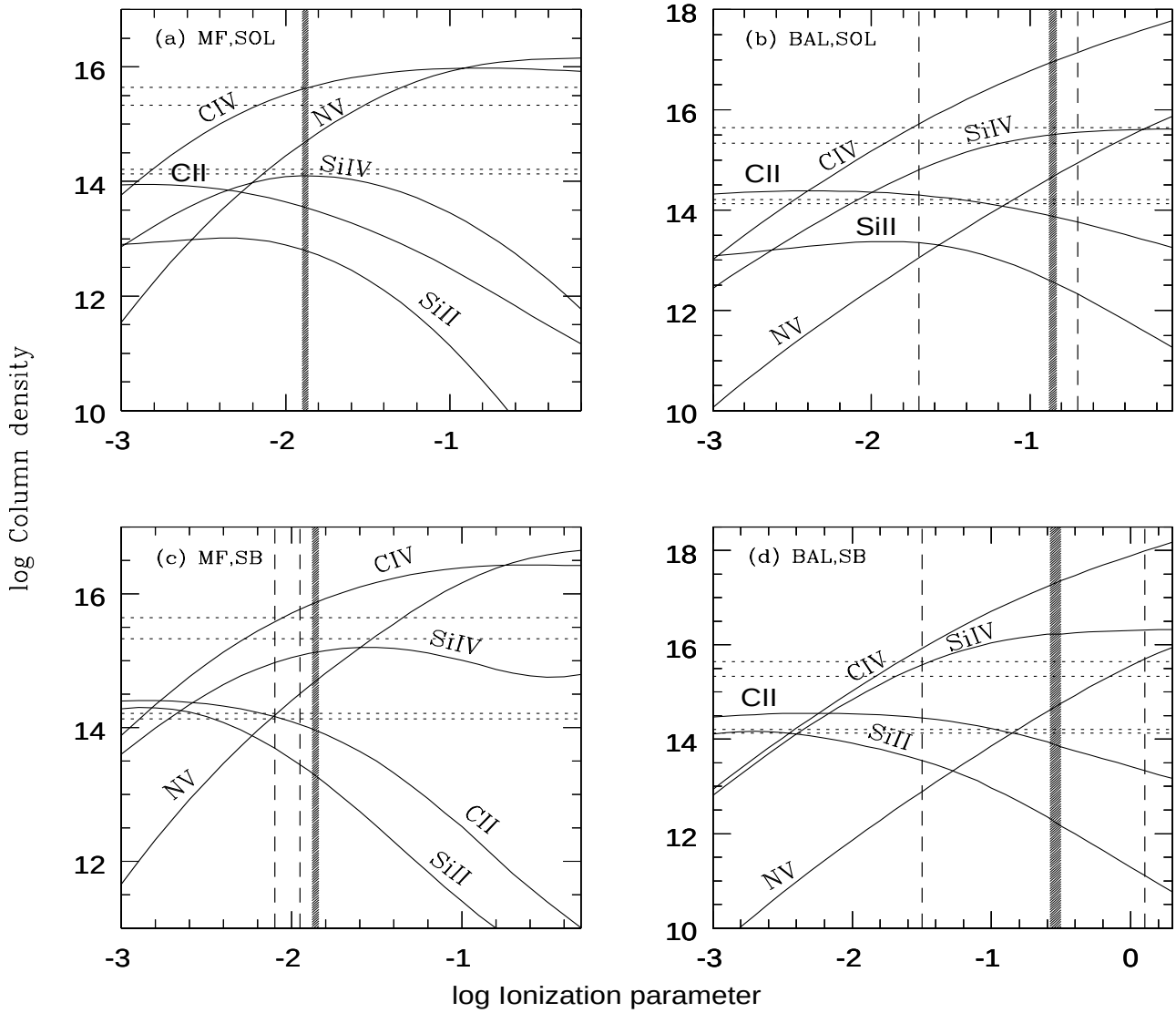

Fig. 7. Predicted column densities of different species as a function of ionization parameter for log N(H I) (cm^{-2}) = 17. Results given in panels **a)** and **b)** are obtained for the MF and BAL spectrum with metallicity 0.1 $Z_{\odot}$. The results for MF and BAL ionizing spectrum with metallicity 1.0 $Z_{\rm SB}$ and 0.5 $Z_{\rm SB}$ of the Starburst enrichment (see Table 2) are given in panels **c)** and **d)** respectively. In each panel the horizontal dotted lines (from bottom to top) mark the limits on the column density of Si II , C II , Si IV and C IV obtained from our observations. While the former two are lower limits the latter two are upper limits. The verticle dashed lines give the limits on the ionization parameters based on the X II/X IV ratios and the observed ratios of N V and Si IV . The verticle shaded region gives the ionization parameter range over which the observed column density of N V is reproduced for the chosen nitrogen metallicity.

which the observed N V column density is reproduced is indicated as a verticle shaded region.

We note that, if the H I column density is close to the observed value (i.e. few 10^{16} cm^{-2}), one needs overall metallicities larger than Solar to explain the observed column densities. We therefore mainly concentrate on models with N(H I) = 10^{17} cm^{-2} that will give a conservative lower limit on the metal enrichment in the system.

If the gas is ionized by a MF type spectrum and has a Solar composition, it can be seen from panel (a) in Fig. 7 that the observed constraints on the ion ratios and the N V and C IV column densities can be consistently reproduced for log $U \simeq -1.9$ (see the shaded region). However the predicted column density of Si IV is lower than the observed value by more than an order of magnitude. It is clear that the observed value can be reproduced only if [Si/H] $\geq$ [Si/H]$_{\odot}$. Increasing the overall abundance actually reduces the required overabundance of Si with respect to N. For example if one assumes $Z = 0.5\,Z_{\odot}$ the observed column densities can be reproduced consistently with lower ionization parameter and a [Si/N] ratio higher than Solar by a factor of 3 only (see Table. 3). Larger metallicities are not possible however as C II would then be detectable.

The enhancement of N(Si IV) with respect to N(N V) can be achieved by either enhancing the silicon metallicity with respect to the nitrogen one as discussed above or by suppressing the N IV ionizing photons. The first possibility can be achieved in a chemical enrichment model where the secondary production of N has not yet begun to dominate.

The latter possibility naturally arise if the cloud sees an attenuated X-ray spectrum, similar to what we observe directly for SDSS J160501.21−011220.0. We explore this possibility in the following.

We model the absorbed spectrum (called BAL spectrum in the following) as the composite of a black body spectrum with temperature $T = 150\,000$ K, plus a power-law spectrum with $\alpha_{uv} = -0.5$ and $\alpha_x = -1.0$ and a relative scaling $\alpha_{\rm ox} = -2.0$. From Fig. 6, it is clear that for a given number of hydrogen ionizing photons this spectrum has less photons to ionize Si III and N IV compared to the MF spectrum. Thus a given ionization state will be produced by higher values of log U and hence higher total hydrogen column densities. However the major difference is the presence of a soft X-ray excess in the MF spectrum that implies more N IV ionizing photons for a given number of Si III ionizing photons compared to the BAL spectrum. For a column density of log N (H I) (cm^{-2}) ≈ 17.00, observations can be reproduced by models with metallicities $0.05\ Z_\odot \leq Z \leq 0.2\ Z_\odot$ (Table 3). This is also demonstrated in panel (b) of Fig. 7. As expected, in these models the results are consistent with observations at an ionization parameter an order of magnitude higher than that required for the MF ionizing spectrum. Thus, we can reproduce the observed column densities with Sub-Solar metallicity and Solar abundance ratios.

It is usual in the case of the BLR clouds to explain an enhanced nitrogen abundance by rapid star formation nucleosynthesis. We consider such a chemical enrichment in our models using option "starburst abundances" in Cloudy (see Table 2). The details of the models are given in Hamann & Ferland (1993). These models have problems in reproducing the observations when a MF ionizing spectrum is considered (see panel (c) in Fig. 7). However, the observed ratios are reproduced if the BAL spectrum is used instead (see Table 3 and panel (d) in Fig. 7) for overall metallicity ≥0.2 and log N(H I) (cm^{-2}) in the range 16 to 17.

It is interesting to note that for all the models considered here the total hydrogen column density is at least an order of magnitude less than the amount required (i.e. N(H(total)) $\geq 5 \times 10^{23}$ cm^{-2}) to explain the lack of X-rays in this QSO by absorption of a standard QSO spectrum (Table 3). We also run models by fixing the total hydrogen column density to be N(H(total)) $\geq 5 \times 10^{23}$ cm^{-2}. For MF ionizing spectrum we do not find any model that can reproduce the constraints noted in Table 1. Thus, we can conclude that either SDSS J160501.21−011220.0 is intrinsically X-ray weak or, if there is any Compton thick screen between the quasar and us, it has nothing to do with the gas that is associated with the red component.

The similar characteristics of the blue component together with the low N(H I) column density of the system strongly suggests that the blue component as well is not Compton thick.

4.2. Formation redshift of the blackhole

We estimate the mass of the black hole from the Eddington accretion. For this we estimate the rest frame luminosity at 2500 Å using the low dispersion spectra obtained by the SDSS group (Fan et al. 2000) to be $L_\nu = 1.37 \times 10^{31}$ erg s^{-1} Hz^{-1}. Applying bolometric correction as suggested by Elvis et al. (1994), we obtain a bolometric luminosity of $L_{\rm bol} = 9.21 \times 10^{46}$ erg s^{-1}. Assuming Eddington accretion we derive the black hole mass, $M_{\rm BH} = 7.1 \times 10^8 \eta^{-1}\ M_\odot$ (see Haiman & Loeb 2001). Here, η is the efficiency parameter (i.e. accretion luminosity given in the units of Eddington luminosity). If $\epsilon = L_{\rm bol}/\dot{M}_{\rm BH}c^2$ is the radiative efficiency for a mass accretion rate $\dot{M}_{\rm BH}$ then the natural e-folding time scale for the growth of a single seed can be written as

$$t = M_{\rm BH}/\dot{M}_{\rm BH} = 4.0 \times 10^7 \epsilon_{0.1} \eta^{-1}\ {\rm yr}. \quad (3)$$

It will therefore take about $\ln(7.1 \times 10^8\, \eta^{-1}\ M_\odot/10\ M_\odot) = 18.1$ e-folding times (or $t \geq 0.7 \epsilon_{0.1} \eta^{-1}$ Gyr) for the black hole to grow to the above estimated mass from a stellar-mass seed of 10 $M_\odot$. For the assumed value of $\epsilon \approx 0.1$ and $\eta \approx 1.0$ this corresponds to a formation epoch of the black hole close to $z \approx 11$ for the cosmological model considered here.

5. Summary

We have presented the analysis of broad absorption lines (BALs) seen in the spectrum of the $z_{\rm em} \simeq 4.92$ QSO SDSS J160501.21-011220.0. Our high spectral resolution UVES spectrum shows two well detached absorption line systems at $z_{\rm abs} = 4.685$ and 4.855. The system at $z_{\rm abs} = 4.855$ covers the background source completely suggesting that the gas is located outside the broad emission line region. On the contrary the system at $z_{\rm abs} = 4.685$, which occults only the continuum source, has a covering factor of the order of 0.9. Physical conditions are investigated in the BAL system at $z_{\rm abs} = 4.855$ using detailed photoionization models. The observed H I column density and the limits on C II and Si II absorptions suggest that log N(H I) (cm^{-2}) is in the range 16–17. The observed column densities of N V , Si IV and C IV in the $z_{\rm abs} = 4.855$ component require, unlike what is derived when analysing broad emission lines, that nitrogen is underabundant by more than a factor of 3 compared to silicon if the gas is photoionized by a typical QSO spectrum. Thus, if the gas is ionized by a standard MF spectrum, the chemical enrichment of the cloud is different from that required by emission line clouds. We show however that the relative supression in the N V column densities can be reproduced for Solar abundance ratios or abundance ratios typical of rapid Starburst nucleosynthesis if we use an ionizing spectrum that is devoid of X-rays. Thus if the composition of BAL is like that of the emission line regions it is most likely that the cloud sees an ionizing spectrum similar to what we observe from this QSO that is strongly attenuated in the X-rays. This is consistent with the fact that none of our models have high enough Compton optical depth to be able to remove X-rays from the QSO. Similar arguments lead to the conclusion that the system at $z_{\rm abs} = 4.685$ as well is not Compton thick.

Using simple Eddington arguments we show that the mass of the central black hole is $\sim 7.1 \times 10^8\ M_\odot$. This suggests that the accretion onto a seed black hole must have started as early as $z \sim 11$. This gives a typical formation epoch for the host galaxy of the QSO.

Acknowledgements. This work was supported in part by the European Communities RTN network "The Physics of the Intergalactic Medium". We wish to thank Dr. Fan for making the low dispersion data on SDSS J160501.21−011220.0 available to us.

References

Ballester, P., Modigliani, A., Boitquin, O., et al. 2000, The Messenger, 101, 31
Becker, R., Fan, X., White, R. L., et al. 2001, AJ, 122, 2850
Blair, A. J., Stewart, G. C., Georgantopoulous, I., et al. 2000, MNRAS, 314, 138
Brandt, W. N., Laor, A., & Wills, B. J. 2000, ApJ, 528, 637
Bregman, J. N. 1984, ApJ, 276, 423
Dekker, H., D'Odorico, S., Kaufer, A., Delabre, B., & Kotzlowski, H. 2000, SPIE, 4008, 534
Dietrich, M., Appenzeller, I., Hamann, F., et al. 2003, A&A, 398, 891
Elvis, M., Wilkes, B. J., McDowell, J. C., et al. 1994, ApJS, 95, 1
Fan, X., Strauss, M. A., Schneider, D. P., et al. 2000, AJ, 119, 1
Ferland, G. J. 1996, HAZY- a brief introduction to Cloudy. Univ.Kentucky, Dept. Physics & Astron. internal report
Gallagher, S., Brandt, W. N., Sambruna, R., Mathur, S., & Yamamski, N. 1999, ApJ, 519, 549
Green, P. J., Aldcroft, T. L., Mathur, S., Wilkes, B. J., & Elvis, M. 2001, ApJ, 558, 109
Green, P. J., & Mathur, S. 1996, ApJ, 462, 637
Haiman, Z., & Loeb, A. 2001, ApJ, 552, 459
Hamann, F. 1997, ApJS, 109, 279
Hamann, F., & Ferland, G. J. 1992, ApJ, 391, L53
Hamann, F., & Ferland, G. J. 1993, ApJ, 418, 11
Hamann, F., & Ferland, G. J. 1999, ARA&A, 37, 487
Korista, K. T., Weymann, R. I., Morris, S. L., et al. 1993, ApJ, 413, 445
Korista, K., Hamann, F., Ferguson, J., & Ferland, G. 1996, ApJ, 461, 641
Kraemer, S. B., Crenshaw, D. M., Yaqoob, T., et al. 2002 [astro-ph/0208478]
Mathews, W. G., & Ferland, G. J. 1987, ApJ, 323, 456
Mathur, S., Elvis, M., & Singh, K. P. 1995, ApJ, 455, 9
Mathur, S., Green, P. J., Arav, N., et al. 2000, ApJ, 533, 79
Matteucci, F., & Padovani, P. 1993, ApJ, 419, 485
Petitjean, P., Rauch, M., & Carswell, R. F. 1994, A&A, 291, 29
Petitjean, P., & Srianand, R. 1999, A&A, 345, 73
Singh, K. P., Westergaard, N. J., & Schnopper, H. W. 1987, A&A, 172, 11
Srianand, R., & Petitjean, P. 2000, A&A, 357, 414
Srianand, R., Petitjean, P., Ledoux, C., & Hazard, C. 2002, MNRAS, 336, 753
Srianand, R., & Shankaranarayanan, S. 1999, ApJ, 518, 672
Turnshek, D. A. 1988, in STScI Symp. Series 2, QSO Absorption lines: Probing the Universe, ed. J. C. Blades, D. Turnshek, & C. Norman (Cambridge: Cambridge Univ. Press)
Verner, D. A., & Barthel, P. D., Tytler, D. 1994, A&AS, 108, 287
Vignali, C., Comastri, A., Cappi, M., et al. 1999, ApJ, 516, 582
Vignali, C., Brandt, W. N., Fan, X., et al. 2001, AJ, 122, 2143
Vignali, C., Brandt, W. N., Schneider, D. P., Garmire, G. P., & Kaspi, S. 2003, AJ, 125, 418
Weymann, R. J., Morris, S. L., Foltz, C. B., & Hewett, P. C. 1991, ApJ, 373, 23